arXiv:hep-ph/9708382v2 27 Nov 1997

Leading logarithmic QCD corrections to the $B_s \to \gamma\gamma$ decays in the two Higgs doublet model

T. M. Aliev ,
International Centre for Theoretical Physics
Trieste, Italy
and
Physics Department, Girne American University
Girne , Cyprus

G. Hiller*,
Deutsches Elektronen-Synchrotron DESY, Hamburg

E. O. Iltan †
Physics Department, Middle East Technical University
Ankara, Turkey

Abstract

We calculate the leading logarithmic QCD corrections to the decay $B_s \to \gamma\gamma$ in the two Higgs doublet model (2HDM) including O_7 type long distance effects and estimate the restrictions of the 2HDM parameters, $tan\beta$ and m_H, using the experimental data of $B \to X_s\gamma$ decay provided by the CLEO Collaboration. A lower bound for the charged Higgs mass m_H as a function of the renormalization scale μ is given for 2HDM model II. We further present the dependencies of the branching ratio $Br(B_s \to \gamma\gamma)$ and the ratio $|A^+|^2/|A^-|^2$ on m_H and $tan\beta$ including leading logarithmic QCD corrections. The dependence on the renormalization scale is found to be strong for both ratios. An additional uncertainty arises from the variation of the parameters of the bound state model, $(m_b, \bar{\Lambda}_s)$. We see, that to look for charged Higgs effects the measurement of the branching ratio $Br(B_s \to \gamma\gamma)$ is promising.

*E-mail address: ghiller@x4u2.desy.de
†E-mail address: eiltan@heraklit.physics.metu.edu.tr

1 Introduction

The experimental discovery of the inclusive and exclusive $B \to X_s\gamma$ [1] and $B \to K^*\gamma$ [2] decays stimulated the study of rare B meson decays as a new force. These decays take place via flavor-changing neutral current (FCNC) $b \to s$ transitions, which are absent in the Standard Model (SM) at tree level and appear only through loops. Therefore, the study of rare B-decays can provide a sensitive test of the structure of the SM at loop level and may shed light on the Kobayashi-Cabibbo-Maskawa (CKM) matrix elements and the leptonic decay constants of the B-mesons. At the same time, such decays are in a very promising class to search for new physics beyond the SM, like two Higgs doublet model (2HDM), minimal supersymmetric model (MSSM), etc. [3]. Currently, the main interest is focused on these decays for which the SM predicts large branching ratio and which can be measured in near future in the constructed B-factories. The $B_s \to \gamma\gamma$ decay belongs to this category. In the SM, the branching ratio of $B_s \to \gamma\gamma$ decay is of order 10^{-7} without QCD corrections. Including leading log (LLog) QCD corrections, the branching ratio (Br) $b \to s\gamma\gamma$ is of the same order of magnitude $\sim 10^{-6}$ like $b \to sl^+l^-$ [4].

The investigation of $B_s \to \gamma\gamma$ decay is interesting for the following reasons:

- It is well-known, that the QCD corrections to the $b \to s\gamma$ decay are considerably large (see [5] - [8] and references therein). Therefore, one can naturally expect that the situation is the same for the $b \to s\gamma\gamma$ decay. Recently the QCD corrections in the LLog approximation to this decay have been calculated and found to be large as expected [9] - [11]. Note, that in the literature this decay without QCD corrections was analysed in the SM [12] - [13] and in the 2HDM [14].

- In $B_s \to \gamma\gamma$ decay, the final photons can be in a CP-odd or a CP-even state. Therefore this decay allows us to study CP violating effects.

- From the experimental point of view, $B_s \to \gamma\gamma$ decay can be easily identified by putting a cut for the energy of the final photons, e.g., the energy of each photon is larger than 100 MeV. In this case, two hard photons will be easily detected in the experiments [15].

- Finally, this decay is also sensitive to the physics beyond the SM.

In an earlier analysis [14], the $Br(B_s \to \gamma\gamma)$ in the 2HDM without QCD corrections was found to be enhanced with respect to the SM one for some values of the parameter space. In the present work, we study $B_s \to \gamma\gamma$ decay in the 2HDM with perturbative QCD corrections in

LLog approximation. In contrast to [14], who used the constituent quark model, we impose a model based on heavy quark effective theory for the bound state of the meson B_s. Further we perform an additional analysis with the inclusion of long-distance effects through the transition $B_s \to \phi\gamma \to \gamma\gamma$, which we call O_7-type throughout this paper, see [9] for details. We find, that the theoretical analysis is shadowed by large uncertainties due to the renormalization scale μ and the parameters of the bound state. The decay $B_s \to \gamma\gamma$ is dominated by the Wilson coefficient C_7^{eff} (see section 2), which is restricted in our analysis by the $B \to X_s\gamma$ branching ratio provided by CLEO data [1], $Br(B \to X_s\gamma) \propto |C_7^{eff}|^2$, see section 3. Without any improvement from the theoretical side, we see that the only chance to detect a deviation from the SM in $B_s \to \gamma\gamma$ decay lies in a possible enhanced branching ratio, which can be at most $1.4 \cdot 10^{-6}$ in the SM [9] and $2.1 \cdot 10^{-6}$ in model II of the 2HDM (for $m_H = 480$ GeV and large $tan\beta$) resulting from our analysis, at $\mu = 2.5$ GeV including the O_7-type long distance effects.

The paper is organized as follows: In Section 2, we give the LLog QCD corrected Hamiltonian responsible for the $b \to s\gamma\gamma$ decay. We further calculate the CP-odd A^- and CP-even A^+ amplitudes in an approach based on heavy quark effective theory, taking the LLog QCD corrections into account. In Section 3, we study the constraint analysis for the 2HDM parameters m_H and $tan\beta$, using the measured data on the branching ratio of the $B \to X_s\gamma$ decay [1]. Section 4 is devoted to an analysis of the dependence of the ratio $|A^+|^2/|A^-|^2$ and the Br on the parameters μ (scale parameter), $tan\beta$ and m_H and our conclusions.

2 Leading logarithmic improved short-distance contributions in the 2HDM for the decay $B_s \to \gamma\gamma$

Before discussing the LLog QCD corrections to the $B_s \to \gamma\gamma$ decay, we would like to remind the main features of the models which we use in further discussions. In the current literature, mainly two types of 2HDM are discussed. In the so-called model I, the up and down quarks get a mass via the vacuum expectation value (v.e.v) of only one Higgs field. In model II, the up and down quarks get mass via v.e.v of the Higgs fields H_1 and H_2, respectively, where H_1 (H_2) corresponds to first (second) Higgs doublet of the 2HDM. Note, that in this sense the Higgs sector of model II coincides with the MSSM extension of the SM. In the 2HDM, there exist five physical Higgs fields, namely, two charged $H^\pm$ and three neutral Higgs bosons. The interaction Lagrangian of the quarks with the charged fields, which we need for the calculation

of the $b \to s\gamma\gamma$ decay amplitude, is [17]

$$\mathcal{L} = \sqrt{\frac{4G_F}{\sqrt{2}}}[m_{u_i}\xi\bar{u}_i L d_j - m_{d_i}\xi'\bar{u}_i L d_j]V_{ij}H^+ + h.c.\ , \tag{1}$$

where L and R denote chiral projections $L(R) = 1/2(1 \mp \gamma_5)$ and ξ and ξ' are the ratios of the two vacuum expectation values, v_1 and v_2 of the Higgs fields H_1 and H_2, respectively. V_{ij} are the elements of the CKM matrix. In model II,

$$\xi' = -1/\xi = -tan\beta = -v_1/v_2\ , \tag{2}$$

and in model I

$$\xi' = \xi = cot\beta = v_2/v_1. \tag{3}$$

After this preliminary remark, let us discuss the LLog QCD corrections to the $b \to s\gamma\gamma$ decay amplitude in the 2HDM. The framework to incorporate short-distance QCD corrections in a systematic way is that of an effective low energy theory with five quarks, namely u,d,s,c,b quarks. The effective Hamiltonian is obtained by integrating out the heavier degrees of freedom, i.e. the top quark, $W^\pm$ and $H^\pm$ bosons. In the effective theory, only the lowest (mass) dimension operators, which are constructed by quark and gauge fields, are taken into account, since higher dimensional operators are suppressed by factors $O(m_b^2/m_t^2)$ and $O(m_b^2/m_W^2)$.

The LLog QCD corrections are done through matching the full theory with the effective theory at the high scale $\mu = m_W$ and then evaluating the Wilson coefficients from m_W down to the lower scale $\mu \sim O(m_b)$. In this way the LLog QCD corrections for the $b \to s\gamma\gamma$ decay in the SM are calculated in [9] - [11].

The effective Hamiltonian relevant for our process is

$$\mathcal{H}_{eff} = -4\frac{G_F}{\sqrt{2}}V_{tb}V_{ts}^*\sum_{i=1}^{8}C_i(\mu)O_i(\mu)\ , \tag{4}$$

where the O_i are operators given in eq. (5) and the C_i are Wilson coefficients renormalized at the scale μ. The coefficients can be calculated perturbatively and the hadronic matrix elements $< V|O_i|B >$ can be calculated using some non-perturbative methods.

The operator basis of $\mathcal{H}_{eff}$ is given as

$$\begin{aligned}
O_1 &= (\bar{s}_{L\alpha}\gamma_\mu b_{L\alpha})(\bar{c}_{L\beta}\gamma^\mu c_{L\beta}),\\
O_2 &= (\bar{s}_{L\alpha}\gamma_\mu b_{L\beta})(\bar{c}_{L\beta}\gamma^\mu c_{L\alpha}),\\
O_3 &= (\bar{s}_{L\alpha}\gamma_\mu b_{L\alpha})\sum_{q=u,d,s,c,b}(\bar{q}_{L\beta}\gamma^\mu q_{L\beta}),
\end{aligned}$$

$$
\begin{aligned}
O_4 &= (\bar{s}_{L\alpha}\gamma_\mu b_{L\beta}) \sum_{q=u,d,s,c,b} (\bar{q}_{L\beta}\gamma^\mu q_{L\alpha}), \\
O_5 &= (\bar{s}_{L\alpha}\gamma_\mu b_{L\alpha}) \sum_{q=u,d,s,c,b} (\bar{q}_{R\beta}\gamma^\mu q_{R\beta}), \\
O_6 &= (\bar{s}_{L\alpha}\gamma_\mu b_{L\beta}) \sum_{q=u,d,s,c,b} (\bar{q}_{R\beta}\gamma^\mu q_{R\alpha}), \\
O_7 &= \frac{e}{16\pi^2}\bar{s}_\alpha \sigma_{\mu\nu}(m_b R + m_s L) b_\alpha \mathcal{F}^{\mu\nu}, \\
O_8 &= \frac{g}{16\pi^2}\bar{s}_\alpha T^a_{\alpha\beta}\sigma_{\mu\nu}(m_b R + m_s L) b_\beta \mathcal{G}^{a\mu\nu},
\end{aligned} \tag{5}
$$

where α and β are $SU(3)$ colour indices and $\mathcal{F}^{\mu\nu}$ and $\mathcal{G}^{\mu\nu}$ are the field strength tensors of the electromagnetic and strong interactions, respectively.

For the reason given below, the LLog QCD corrections can be calculated in analog to the SM. In the 2HDM, the charged Higgs fields are present and give new contributions due to the their exchange diagrams. Since the interaction vertices of the charged Higgs bosons and quarks are proportional to the ratio m_q/m_W, where m_q is the mass of the quark and m_W is the mass of the W boson, the main contribution comes from the interaction with the t-quark. We neglect the contributions coming from u and c quarks, since their masses are negligibly small compared to m_W. In this case the calculations show, that the new contributions modify only the Wilson coefficients C_7 and C_8 of the operators O_7 and O_8 at m_W scale and do not bring any new operators [14]. Therefore the operator basis used in the 2HDM is the same as the basis used in the SM for the $b \to s\gamma\gamma$ decay.

Denoting the Wilson coefficients for the SM with $C_i^{SM}(m_W)$ and the additional charged Higgs contribution with $C_i^H(m_W)$, we have the initial values [18]:

$$
\begin{aligned}
C^{SM}_{1,3,\ldots 6}(m_W) &= 0\ , \\
C^{SM}_{2}(m_W) &= 1\ , \\
C^{SM}_{7}(m_W) &= \frac{3x^3-2x^2}{4(x-1)^4}\ln x + \frac{-8x^3-5x^2+7x}{24(x-1)^3}\ , \\
C^{SM}_{8}(m_W) &= -\frac{3x^2}{4(x-1)^4}\ln x + \frac{-x^3+5x^2+2x}{8(x-1)^3}\ ,
\end{aligned} \tag{6}
$$

and [14], [16]

$$
\begin{aligned}
C^{H}_{1,\ldots 6}(m_W) &= 0\ , \\
C^{H}_{7}(m_W) &= \xi\xi'[\frac{-3y^2+2y}{6(y-1)^3}\ln y + \frac{3y-5y^2}{12(y-1)^2}]\ , \\
&+ \xi^2[\frac{3y^3-2y^2}{12(y-1)^4}\ln y + \frac{-8y^3-5y^2+7y}{72(y-1)^3}]\ ,
\end{aligned}
$$

$$
\begin{aligned}
C_8^H(m_W) &= \xi\xi'[\frac{y}{2(y-1)^3}\ln y + \frac{y^2-3y}{4(y-1)^2}] \ , \\
&+ \xi^2[\frac{y^2}{4(y-1)^4}\ln y + \frac{-y^3+5y^2+2y}{24(y-1)^3}] \ , \qquad (7)
\end{aligned}
$$

where $x = m_t^2/m_W^2$ and $y = m_t^2/m_H^2$. Here the parameters ξ and ξ' are given in eqs. (2) and (3). From eqs. (6) and (7) the initial values of the coefficients for the 2HDM are defined as:

$$
\begin{aligned}
C_{1,3,...6}^{2HDM}(m_W) &= 0 \ , \\
C_2^{2HDM}(m_W) &= 1 \ , \\
C_7^{2HDM}(m_W) &= C_7^{SM}(m_W) + C_7^H(m_W) \ , \\
C_8^{2HDM}(m_W) &= C_8^{SM}(m_W) + C_8^H(m_W). \qquad (8)
\end{aligned}
$$

Using the initial values of the Wilson coefficients C_i^{2HDM}, we can calculate their contributions at any lower scale as in the SM case. Here we would like to make the following remark: Since in our case there exists a charged Higgs boson with a mass larger than m_W, the correct procedure to calculate the Wilson coefficients at a lower scale μ has two stages: First, we calculate the value at m_W starting from m_H and second, we evaluate the result from m_W down to a lower scale μ. We assume that the evaluation from m_H to m_W gives a negligible contribution to the Wilson coefficients and therefore we consider only their evaluation between m_W and a lower scale μ.

Using the effective Hamiltonian in eq. (4), the amplitude for the decay $B_s \to \gamma\gamma$ can be written as [9] - [14]

$$
\mathcal{A}(B_s \to \gamma\gamma) = A^+ \mathcal{F}_{\mu\nu}\mathcal{F}^{\mu\nu} + iA^- \mathcal{F}_{\mu\nu}\tilde{\mathcal{F}}^{\mu\nu} \ , \qquad (9)
$$

where $\tilde{\mathcal{F}}_{\mu\nu} = \frac{1}{2}\epsilon_{\mu\nu\alpha\beta}\mathcal{F}^{\alpha\beta}$. Here A^+ (A^-) is the CP-even (CP-odd) part in a HQET inspired approach [9] :

$$
\begin{aligned}
A^+ &= \frac{\alpha_{em}G_F}{\sqrt{2}\pi}\frac{f_{B_s}}{m_{B_s}^2}\lambda_t\left(\frac{1}{3}\frac{m_{B_s}^4(m_b^{eff}-m_s^{eff})}{\bar{\Lambda}_s(m_{B_s}-\bar{\Lambda}_s)(m_b^{eff}+m_s^{eff})}C_7^{eff}(\mu)\right. \\
&- \left.\frac{4}{9}\frac{m_{B_s^2}}{m_b^{eff}+m_s^{eff}}(-m_b J(m_b)+m_s J(m_s))D(\mu)\right), \\
A^- &= -\frac{\alpha_{em}G_F}{\sqrt{2}\pi}f_{B_s}\lambda_t\left(\frac{1}{3}\frac{1}{m_{B_s}\bar{\Lambda}_s(m_{B_s}-\bar{\Lambda}_s)}g_- C_7^{eff}(\mu)\right. \\
&- \left.\sum_q Q_q^2 I(m_q)C_q(\mu) + \frac{1}{9(m_b^{eff}+m_s^{eff})}(m_b\triangle(m_b)+m_s\triangle(m_s))D(\mu)\right) \ , \qquad (10)
\end{aligned}
$$

where $Q_q = \frac{2}{3}$ for $q = u, c$ and $Q_q = -\frac{1}{3}$ for $q = d, s, b$. In the calculations, we have used the unitarity of the CKM-matrix $\sum_{i=u,c,t} V_{is}^* V_{ib} = 0$ and have neglected the contribution due to

$V_{us}^* V_{ub} \ll V_{ts}^* V_{tb} \equiv \lambda_t$. The function g_- is defined as:

$$g_- = m_{B_s}(m_b^{eff} + m_s^{eff})^2 + \bar{\Lambda}_s(m_{B_s}^2 - (m_b^{eff} + m_s^{eff})^2) \ . \tag{11}$$

The parameter $\bar{\Lambda}_s$ enters eq. (10) through the bound state kinematics [9]. m_b^{eff} and m_s^{eff} are the effective masses of the quarks in the B_s meson bound state [9],

$$\begin{aligned} (m_b^{eff})^2 &= p^2 = m_b^2 - 3\lambda_2 \ , \\ (m_s^{eff})^2 &= p'^2 = (m_s^{eff})^2 - m_{B_s}^2 + 2m_{B_s}\bar{\Lambda}_s \ , \end{aligned} \tag{12}$$

where λ_2 comes from the matrix element of the heavy quark expansion [19]. The LLog QCD-corrected Wilson coefficients $C_{1\ldots6}(\mu)$ [9] - [11] enter the amplitudes in the combinations

$$\begin{aligned} C_u(\mu) &= C_d(\mu) = (C_3(\mu) - C_5(\mu))N_c + C_4(\mu) - C_6(\mu) \ , \\ C_c(\mu) &= (C_1(\mu) + C_3(\mu) - C_5(\mu))N_c + C_2(\mu) + C_4(\mu) - C_6(\mu) \ , \\ C_s(\mu) &= C_b(\mu) = (C_3(\mu) + C_4(\mu))(N_c + 1) - N_c C_5(\mu) - C_6(\mu) \ , \\ D(\mu) &= C_5(\mu) + C_6(\mu)N_c \ , \end{aligned} \tag{13}$$

where N_c is the number of colours ($N_c = 3$ for QCD). While $C_{1\ldots6}(\mu)$ are the coefficients of the operators $O_{1\ldots6}$, $C_7^{eff}(\mu)$ is the "effective" coefficient of O_7 and contains renormalization scheme dependent contributions from the four-quark operators $O_{1\ldots6}$ in $\mathcal{H}_{eff}$ to the effective vertex in $b \to s\gamma$. In the NDR scheme, which we use here, $C_7^{eff}(\mu) = C_7(\mu) - \frac{1}{3}C_5(\mu) - C_6(\mu)$, see [18] for details. The functions $I(m_q)$, $J(m_q)$ and $\triangle(m_q)$ come from the irreducible diagrams with an internal q type quark propagating and are defined as

$$\begin{aligned} I(m_q) &= 1 + \frac{m_q^2}{m_{B_s}^2}\triangle(m_q) \ , \\ J(m_q) &= 1 - \frac{m_{B_s}^2 - 4m_q^2}{4m_{B_s}^2}\triangle(m_q) \ , \\ \triangle(m_q) &= \left(\ln(\frac{m_{B_s} + \sqrt{m_{B_s}^2 - 4m_q^2}}{m_{B_s} - \sqrt{m_{B_s}^2 - 4m_q^2}}) - i\pi\right)^2 \text{ for } \frac{m_{B_s}^2}{4m_q^2} \geq 1, \\ \triangle(m_q) &= -\left(2\arctan(\frac{\sqrt{4m_q^2 - m_{B_s}^2}}{m_{B_s}}) - \pi\right)^2 \text{ for } \frac{m_{B_s}^2}{4m_q^2} < \ 1. \end{aligned} \tag{14}$$

In our numerical analysis we used the input values given in Table (1).

Parameter	Value
m_c	1.4 (GeV)
m_b	4.8 (GeV)
α_{em}^{-1}	129
λ_t	0.04
$\Gamma_{tot}(B_s)$	$4.09 \cdot 10^{-13}$ (GeV)
f_{B_s}	0.2 (GeV)
m_{B_s}	5.369 (GeV)
m_t	175 (GeV)
m_W	80.26 (GeV)
m_Z	91.19 (GeV)
$\Lambda_{QCD}^{(5)}$	0.214 (GeV)
$\alpha_s(m_Z)$	0.117
λ_2	0.12 (GeV^2)

Table 1: Values of the input parameters used in the numerical calculations unless otherwise specified.

3 Constraint analysis

There is a considerable interest in the constraints of the parameter space of the 2HDM, especially in model II, since its Higgs sector coincides with the minimal supersymmetric extension of the SM one. The free parameters of the 2HDM are the masses of the charged and neutral Higgs bosons and the ratio of the v.e.v. of the two Higgs fields, denoted by $\tan\beta$. In our analysis the neutral Higgs bosons are irrelevant, since they do not give any contribution to the $b \to s\gamma\gamma$ process. Therefore we consider as free parameters the mass m_H of the charged Higgs boson and $tan\beta$. By using existing experimental data, it is possible to find restrictions on the parameters m_H and $tan\beta$.

The model independent lower bound of the mass of the charged Higgs $m_H \geq 44\ GeV$ comes from the non-observation of charged H pairs in Z decays [20]. There are no experimental upper bounds for m_H except $m_H \leq 1\ TeV$ to satisfy the unitarity condition [21]. For model II, the constraints have already been studied. Top decays give $m_H \geq 147\ GeV$ for large $tan\beta$ [22]. The lower bound of $tan\beta$ is found to be 0.7 due to the decay $Z \to b\bar{b}$ [23] and in addition for large $tan\beta$ the ratio $tan\beta/m_H$ is restricted. The current limits are $tan\beta/m_H \leq 0.38\ GeV^{-1}$ [24] and $tan\beta/m_H \leq 0.46\ GeV^{-1}$ [25], which come from the experimental results of branching ratios of the decays $B \to \tau\bar{\nu}$ and $B \to X\tau\bar{\nu}$. Recently, the exclusive decay mode $B \to D\tau\bar{\nu}$ has been studied [26] for model II. It was shown that this decay could be used to put an upper bound on $tan\beta/m_H$, with the sufficient data and the reduction of theoretical uncertainities.

Under these conditions, the upper bound was estimated as $tan\beta/m_H = 0.06\ GeV^{-1}$.

In the present work, we estimate the constraints for the 2HDM parameters using the result coming from the measurement of the decay $B \to X_s\gamma$ by the CLEO collaboration [1]:

$$Br(B \to X_s\gamma) = (2.32 \pm 0.57 \pm 0.35) \cdot 10^{-4}. \tag{15}$$

To reduce the b-quark mass dependence let us consider the ratio

$$\begin{aligned} R &= \frac{Br(B \to X_s\gamma)}{Br(B \to X_c e\bar{\nu}_e)} \\ &= \frac{|V_{ts}^* V_{tb}|^2}{|V_{cb}|^2} \frac{6\alpha_{em}}{\pi g(z)} |C_7^{eff}|^2 \ , \end{aligned} \tag{16}$$

where $g(z)$ is the phase space factor in semileptonic b-decay,

$$g(z) = 1 - 8z^2 + 8z^6 + z^8 - 24z^4 ln\, z \tag{17}$$

and $z = m_c/m_b$.

Now we want to discuss the theoretical uncertainties present in the prediction of R.

- The ratio of the CKM matrix elements $\frac{|V_{ts}^* V_{tb}|^2}{|V_{cb}|^2} = 0.95 \pm 0.04$ has an uncertainty which comes from the CP violating parameter ϵ_κ [8].

- The function $g(z)$ has an uncertainty coming from the masses m_b and m_c via the ratio $z = m_c/m_b$. HQET provides a mass relation [27]

$$m_b - m_c = (m_{\bar{B}} - m_{\bar{D}})[1 - \frac{\lambda_1}{2m_B m_D} + O(\frac{1}{m_Q^3})] \ , \tag{18}$$

  where $Q = b$ and c , $m_{\bar{B}}$ and $m_{\bar{D}}$ are spin averaged meson masses, $m_{\bar{B}} = 5.31\ GeV$ and $m_{\bar{D}} = 1.97\ GeV$ [27]. Here λ_1 is the non-perturbative parameter, which characterizes the average kinetic energy of the b-quark in B meson and its value is obtained by QCD sum rules. Using the theoretical estimate for $\lambda_1 = -(0.4 \pm 0.2)\ GeV^2$ [28], the mass difference and the error quoted are given as

$$m_b - m_c = (3.40 \pm 0.03 \pm 0.03)\ GeV. \tag{19}$$

  Here the first error is due to the uncertainty in λ_1 and the second one is from higher order corrections. We take the central value of b-quark mass as $m_b = 4.8\ GeV$. The uncertainty in m_b is $\Delta m_b = \pm 0.1\ GeV$. Using the HQET result, we estimate the uncertainty in m_c as $\Delta m_c = \pm 0.16$ and we get the error in $g(\bar{z})$ as $\Delta g(\bar{z}) = 0.096$ and $\Delta g(\bar{z})/g(\bar{z}) = 17.8\ \%$, where $\bar{z} = m_c/m_b = 0.29$ is the central value.

The Br for the semileptonic $B \to X_c e \bar{\nu}_e$ is [29]

$$Br(B \to X_c e \bar{\nu}_e) = 0.103 \pm 0.01. \tag{20}$$

Both the theoretical uncertainties and the experimental errors, as given in eq. (15) and (20), result in an uncertainty in C_7^{eff}. Using

$$\begin{aligned} Br_{max}(B \to X_s \gamma) &= 3.24 \cdot 10^{-4} \ , \\ Br_{min}(B \to X_s \gamma) &= 1.40 \cdot 10^{-4} \ , \end{aligned} \tag{21}$$

we get a possible range for $|C_7^{eff}|$ as

$$0.1930 \leq |C_7^{eff}| \leq 0.4049 \ . \tag{22}$$

In the SM and 2HDM model II is $C_7^{eff} < 0$, but in possible extensions it can be positive.

Now we present the lower bounds of m_H for different values of the scale μ in Table (2) for model II. We restricted $|C_7^{eff,2HDM}(\mu)|$ by using the limits given in eq. (22). For model I, a

m_{Hmin} $[GeV]$	μ $[GeV]$
480	2.5
302	5
235	10
158	m_W

Table 2: The lower bounds of the Higgs mass m_H for different scales μ in model II.

lower bound for the Higgs boson mass is absent.

The parameter $tan\beta$ has bounds strongly depending on the scale μ and m_H. In fig. (1), we plot the parameter $tan\beta$ with respect to m_H for 3 different μ scales (2.5, 5, 10) GeV in model II, by fixing $|C_7^{eff,2HDM}| = 0.4049$. We see, that the dependence of $tan\beta$ (m_H) on m_H ($tan\beta$) becomes weak for large values of m_H ($tan\beta$) and that a decreasing μ scale causes the allowed region in the $tan\beta$ - m_H plane is to be small. It is interesting that at $\mu = 2.5\ GeV$, the solution for $tan\beta$ - m_H exists only in the region $0.4047 \leq |C_7^{eff,2HDM}| \leq 0.4049$. Therefore the solid curve in Fig (1) is almost the allowed region for $(tan\beta, m_H)$. For $\mu = 2.5\ GeV$, we get an empirical expression for the restricted region of the parameter set $(tan\beta, m_H)$,

$$tan\beta = c_1 + \frac{c_2}{\sqrt{m_H - m_p}} \ , \tag{23}$$

with $c_1 = -0.067$, $c_2 = 6.9\ GeV^{1/2}$ and $m_p = m_{H\,min} - \epsilon$. Here ϵ is a positive small number ($\epsilon \ll 1$) and $m_{H\,min} = 480\ GeV$.

In the following analysis we restrict the coefficient $|C_7^{eff,2HDM}|$ in the given region and study the resulting m_H, $tan\beta$ and scale μ dependencies of the ratio $|A^+|^2/|A^-|^2$ and the Br for the decay $B_s \to \gamma\gamma$.

4 Discussion

In the rest frame of the B_s meson, the $CP = -1$ amplitude A^- is proportional to the perpendicular spin polarization $\vec{\epsilon_1} \times \vec{\epsilon_2}$, and the $CP = 1$ amplitude A^+ is proportional to the parallel spin polarization $\vec{\epsilon_1}.\vec{\epsilon_2}$. The ratio $|A^+|^2/|A^-|^2$ is informative to search for CP violating effects in $B_s \to \gamma\gamma$ decays and it has been studied before in the literature in the framework of the 2HDM without QCD corrections [14]. In our analysis we use three sets of parameters $(m_b, \bar{\Lambda}_s)$ given in (Table (3)), which model the bound state [9]. However, we do not present the figures for the first two. Here we analyze the LLog μ, and 2HDM parameters (m_H, $tan\beta$) dependence of the ratio $|A^+|^2/|A^-|^2$ and present the results in a series of graphs (fig. 2-7).

In fig. (2) and (3) we plot the dependence of $|A^+|^2/|A^-|^2$ on m_t/m_H for fixed $tan\beta = 2$ and four different μ scales, (m_W, 10, 5, 2.5) GeV in model II and model I, respectively. Decreasing the scale μ weakens the dependence of the ratio $|A^+|^2/|A^-|^2$ on m_H and the contribution of the charged Higgs bosons to $|A^+|^2/|A^-|^2$ gets small. The lower limit of the Higgs mass is sensitive to the scale μ and it increases with decreasing μ in model II, (Table (2)). However, the Higgs mass has no lower bound in model I.

Fig. (4) and (5) show the dependence of $|A^+|^2/|A^-|^2$ on $tan\beta$ for fixed $m_H = 500\ GeV$. This ratio is sensitive only to small $tan\beta$ values. The μ scale regulates the lower limit of $tan\beta$ for model I and model II in an opposite way. Further, the effect of the charged Higgs contribution becomes weak for large $tan\beta$ values.

In fig. (6) and (7) we present the μ scale dependence of $|A^+|^2/|A^-|^2$ for the SM and 2HDM with $tan\beta = 10$ and two different mass values $m_H = 500\ GeV,\ 800\ GeV$ for model II and model I, respectively. We find, that for model II the smaller the value of m_H, the less dependent is the ratio on μ. Model I does not allow us to discriminate between the SM or different values of m_H used as expected (see e.g. fig. (5)).

set 1	*set* 2	*set* 3
$\Lambda_s = 370$ MeV	$\Lambda_s = 480$ MeV	$\Lambda_s = 590$ MeV
$m_b = 5.03$ GeV	$m_b = 4.91$ GeV	$m_b = 4.79$ GeV

Table 3: The parameter sets of the bound state model, $(m_b, \bar{\Lambda}_s)$.

The lowest order result of $|A^+|^2/|A^-|^2$ in α_s is obtained by setting $\mu = m_W$ and it is 0.30 in the SM for set 3. It reaches 0.85 at $\mu = 2.5\ GeV$. Varying μ in the range 2.5 GeV $\leq \mu \leq$ 10.0 GeV, $|A^+|^2/|A^-|^2$ is changing in the range $0.60 \ \leq |A^+|^2/|A^-|^2 \leq 0.85$, resulting in an uncertainty of $\frac{\triangle(|A^+|^2/|A^-|^2)}{(|A^+|^2/|A^-|^2)(\mu=5\ GeV)} \approx \pm 35\%$ in the SM. Now we give an example to compare the dependence of the ratio $|A^+|^2/|A^-|^2$ on the scale μ and the 2HDM parameters: In model II, for $m_H = 500\ GeV$ and $tan\beta \geq 2$, the lowest order result of the ratio $|A^+|^2/|A^-|^2$ is 0.40 and it enhances up to 0.50 with decreasing $tan\beta$. However, at $\mu = 2.5\ GeV$ the ratio reaches 0.86 and the uncertainty due to the extended Higgs sector is weaker than the one due to the scale μ. In model I, the behaviour is the same.

This shows, that the ratio $|A^+|^2/|A^-|^2$ is quite sensitive to QCD corrections and this strong μ dependence makes the analysis of the 2HDM parameters m_H and $tan\beta$ for the given experimental value of the ratio $|A^+|^2/|A^-|^2$ difficult. However, we believe, that the strong μ dependence will be reduced with the addition the of next to leading order (NLO) calculation, and the analysis on the parameters will be more reliable. Note, that a similar analysis for the decay $b \to s\gamma$ is given in [6], [8].

In addition, there is another uncertainty due to the different parameter sets (Table (3)). For set 2 $|A^+|^2/|A^-|^2 = 0.36$ and for set 1 $|A^+|^2/|A^-|^2 = 0.40$ in the SM and in the lowest order of α_s. It follows, that the larger m_b (smaller $\bar{\Lambda}_s$), the larger the ratio. We further see that having increased m_b, the ratio $|A^+|^2/|A^-|^2$ becomes less sensitive to the scale μ. This ratio essentially changes when QCD corrections are taken into account. In the lowest order of α_s, A^+ and A^- depend both on the one particle reducible part (IPR), proportional to $C_7^{eff} = C_7$ and in addition A^- contains the one particle irreducible part (IPI), proportional to C_2, see eq. (10). If we include QCD corrections to the considered ratio, the contribution of C_7^{eff} dominates over the IPI sector and the value of the ratio increases. This means, that the values of A^+ and A^- come close to each other and it can be explained as a cancellation of the IPI sector.

Now we continue to analyze the Br displayed in a series of figures 8-13. In fig. 8-11, we present the $\frac{m_t}{m_H}$ and $tan\beta$ dependencies of the Br. Decreasing m_H, the Br increases in model II, however, the behaviour is opposite in model I. On the other hand the Br is sensitive to small $tan\beta$. For large values of $tan\beta$, the dependence of the Br on $tan\beta$ becomes weak in model II. In model I, the 2HDM result almost coincides with the SM one since the charged Higgs contribution is proportional to $1/(tan\beta)^2$. Similar to the case of $|A^+|^2/|A^-|^2$, the Br is strongly dependent on the scale μ, see figs (12-13)). It is enhanced for small values of μ. For parameter set 3, the lowest order result is $3.6 \cdot 10^{-7}$ in the SM. It increases up to $6.8 \cdot 10^{-7}$

at $\mu = 2.5\ GeV$. Varying μ in the range 2.5 GeV $\leq \mu \leq$ 10.0 GeV, the Br changes between $5.0 \cdot 10^{-7} \leq Br \leq 6.9 \cdot 10^{-7}$, and this gives an uncertainty $\triangle Br/Br(\mu = 5\text{ GeV}) \approx \pm 30\%$ for the SM. For set 1 (2), the Br increases up to $1.7 \cdot 10^{-6}$ $(1.0 \cdot 10^{-6})$ and the uncertainty is also increases, as due to the scale μ dependence, namely 39 (35) %. This behaviour of the Br results mainly from the $1/\bar{\Lambda}_s$ dependence in amplitudes.

With the addition of extra Higgs contribution, the uncertainty due to 2HDM parameters m_H and $tan\beta$ in the Br becomes large like the one coming from the scale μ. Now we will give an example to see the effect of the 2HDM parameters on the Br by choosing set 3. In model II for $m_H = 500\ GeV$, the lowest order result of the Br is $5.8 \cdot 10^{-7}$ for $tan\beta \geq 2$ (see fig. 10) and it reaches $1.1 \cdot 10^{-6}$ for smaller $tan\beta$. For comparison, the value in the SM is $3.6 \cdot 10^{-7}$. At $\mu = 2.5\ GeV$ the Br reaches $6.9 \cdot 10^{-7}$ $(9.0 \cdot 10^{-7})$ in the SM (2HDM).. This shows, that the Br is also sensitive to the extra Higgs contribution. For $m_H = 500\ GeV$ and $\mu = 2.5\ GeV$, the Br in the 2HDM model II is enhanced $\sim 30\%$ compared to the SM. In model I, there is a suppression due to the extra Higgs contribution compared to the SM (see fig. (11)), however, the Br is still sensitive to the scale μ (see fig. (13)) and the 2HDM parameters.

We complete this section by taking the O_7 type long distance effects (LD_{O_7}) for both the ratio $|A^+|^2/|A^-|^2$ and the Br into account. The LD_{O_7} contribution to the CP-odd A^- and CP-even A^+ amplitudes has recently been calculated with the help of the Vector Meson Dominance model (VMD) [9] and it was shown, that the influence on the amplitudes is destructive. With the addition of the LD_{O_7} effects, the amplitudes entering $|A^+|^2/|A^-|^2$ and the Br are now given as

$$\begin{aligned} A^+ &= A^+_{SD} + A^+_{LD_{O_7}}\ , \\ A^- &= A^-_{SD} + A^-_{LD_{O_7}}\ , \end{aligned} \tag{24}$$

where $A^\pm_{SD}$ are the short distance amplitudes we took into account in the previous sections (eq. 10). The LD_{O_7} amplitudes $A^\pm_{LD_{O_7}}$ are defined as [9]

$$\begin{aligned} A^+_{LD_{O_7}} &= -\sqrt{2}\frac{\alpha_{em} G_F}{\pi}\bar{F}_1(0) f_\phi(0)\lambda_t \frac{m_b(m^2_{B_s} - m^2_\phi)}{3 m_\phi m^2_{B_s}} C_7^{eff}(\mu)\ , \\ A^-_{LD_{O_7}} &= \sqrt{2}\frac{\alpha_{em} G_F}{\pi}\bar{F}_1(0) f_\phi(0)\lambda_t \frac{m_b}{3 m_\phi} C_7^{eff}(\mu)\ , \end{aligned} \tag{25}$$

where $f_\phi(0) = 0.18\ GeV$ is the decay constant of ϕ meson at zero momentum, $\bar{F}_1(0)$ is the extrapolated $B_s \to \phi$ form factor (for details see [9]).

In fig. (14 - 19) we present the m_H, $tan\beta$ and μ dependencies of the ratio $|A^+|^2/|A^-|^2$ and the Br with the addition of LD_{O_7} effects for set 3. Here we use $\bar{F}_1(0) = 0.16$ [9]. It

can be shown, that the value of the ratio $|A^+|^2/|A^-|^2$ decreases with the addition of LD_{O_7} effects. However, while the scale μ is decreasing, the effect of the LD_{O_7} contribution on the ratio $|A^+|^2/|A^-|^2$ is also decreasing, see fig. 4 and 15. On the other hand, the uncertainty resulting from varying μ between 2.5 GeV $\leq \mu \leq$ 10.0 GeV has increased compared to the case without the inclusion of the LD_{O_7} amplitudes:

$$\frac{\triangle(|A^+|^2/|A^-|^2)}{(|A^+|^2/|A^-|^2)(\mu = 5 \text{ GeV})} \approx \pm 40\% \ .$$

The Br decreases with the addition of LD_{O_7} effects, since the effect is destructive. The μ scale uncertainty of the Br is smaller compared to the case where no LD effect is included and we get for the range 2.5 GeV $\leq \mu \leq$ 10.0 GeV in the SM

$$\frac{\triangle Br}{Br(\mu = 5 \text{ GeV})} \approx \pm 27\% \ . \tag{26}$$

The present experimental limit on the decay $B_s \to \gamma\gamma$ is [30]

$$Br(B_s \to \gamma\gamma) \leq 1.48 \cdot 10^{-4} \ , \tag{27}$$

which is far from the theoretical results. By varying the parameters $\mu, m_H, tan\beta, (m_b, \bar{\Lambda}_s)$, it is possible to enhance the Br up to $2.1\,(2.5) \cdot 10^{-6}$ in model II for $m_H = 480$ GeV and large $tan\beta$, where the possible maximal value in the SM is $1.4\,(1.7) \cdot 10^{-6}$, both at $\mu = 2.5$ GeV and for set 1. The numbers in parentheses correspond to the case where no LD_{O7} effects are taken into account.

LLog calculations show that the Br strongly depends on the scale μ. This strong dependence will disappear with the addition of NLO QCD corrections. From NLO $b \to s\gamma$ decay, the choice of $\mu = m_b/2$ in the LLog expression reproduces effectively the NLO result, so one suggest that this may work also for the $b \to s\gamma\gamma$ decay. An additional theoretical uncertainty arises from the poor knowledge of the B_s bound state effects.

We find that the Br increases with the addition of the extra Higgs contribution and even at the scale $\mu = 2.5\,GeV$ this value is $\sim$ 2 orders of magnitude smaller than the present experimental upper bound. The other possibility for an enhancement of the Br is the extension of the Higgs sector. This forces us to think of further models like MSSM,...etc. and FCNC $B_s \to \gamma\gamma$ decay will be an efficient tool to search for new physics beyond the SM.

Acknowledgements

One of the authors (T. M. A) would like to thank International Centre for Theoretical Physics (ICTP) for the warm hospitality. He also acknowleges Prof.S.Randjbar-Daemi for his interest and support.

References

[1] M. S. Alam et al., CLEO Collaboration, Phys. Rev. Lett. **74** (1995) 2885.

[2] R. Ammar et al., CLEO Collaboration, Phys. Rev. Lett **71** (1993) 674.

[3] J. L. Hewett, in proc. of the 21^{st} Annual SLAC Summer Institute, ed. L. De Porcel and C. Dunwoode, SLAC-PUB6521.

[4] A. Ali, L.T. Handoko, G. Hiller and T. Morozumi, Phys. Rev. D **55** (1997) 4105.

[5] B. Grinstein, R. Springer, and M. Wise, Nucl. Phys. B**339** (1990) 269; R. Grigjanis, P.J. O'Donnel, M. Sutherland and H. Navelet, Phys. Lett. B**213** (1988) 355; Phys. Lett. B**286** (1992) E, 413; G. Cella, G. Curci, G. Ricciardi and A. Viceré, Phys. Lett. B**325** (1994) 227, Nucl. Phys. B**431** (1994) 417; M. Misiak, Nucl. Phys B**393** (1993) 23, Erratum B**439** (1995) 461.

[6] K. G. Chetyrkin, M. Misiak and M. Münz, hep-ph/9612313; C. Greub, T. Hurth and D. Wyler, Phys. Lett.B **380** (1996) 385; Phys. Rev. D **54** (1996) 3350.

[7] M. Ciuchini, E. Franco, G. Martinelli, L. Reina and L. Silvestrini, Phys. Lett. B**316** (1993) 127; Nucl. Phys. B**421** (1994) 41.

[8] A. J. Buras, M. Misiak, M. Münz and S. Pokorski, Nucl. Phys. B**424** (1994) 374.

[9] G. Hiller and E. Iltan, Phys. Lett B **409** (1997) 425.

[10] C. H. V. Chang, G. L. Lin and Y. P. Yao, hep-ph/9705345.

[11] L. Reina, G. Riccardi and A. Soni, Phys. Rev. D **56** (1997) 5805.

[12] G.-L. Lin, J. Liu and Y.-P. Yao, Phys. Rev. Lett. **64** (1990) 1498;
G.-L. Lin, J. Liu and Y.-P. Yao, Phys. Rev. D **42** (1990) 2314.

[13] H. Simma and D. Wyler, Nucl. Phys. B **344** (1990) 283.

[14] T. M. Aliev and G. Turan, Phys. Rev. D **48** (1993) 1176.

[15] L. Reina, G. Riccardi and A. Soni,Phys. Lett B **396** (1997) 231.

[16] B. Grinstein, M. Savage and M. B. Wise, Nucl. Phys. B **319** (1989) 271.

[17] L. F. Abott, P. Sikivie and M. B. Wise, Phys. Rev. D**21** (1980) 1393.

[18] A. Ali and C. Greub, Z. Phys. C **49** (1991) 431;
A. J. Buras et al., Nucl. Phys. B **424** (1994) 374.

[19] A. Manohar and M. B. Wise, Phys. Rev. D **49** (1994) 1310.

[20] P. Abreu et al., Z. Phys. C **64** (1994) 183;
G. Alexander et al., Phys. Lett. B **370** (1996) 174.

[21] M. Veltman, Acta Phys. Polon. B **8** (1977) 475;
B. W. Lee, C. Quigg, H. B. Thacker, Phys. Rev. D **16** (1977) 253;
M. Veltman, Phys. Lett. B **70** (1977) 253.

[22] F. Abe et al., hep-ex/9704003.

[23] A. K. Grant, Phys. Rev. D **51** (1995) 207.

[24] M. Acciari et al., Phys. Lett. D **396** (1997) 327.

[25] ALEPH Collaboration, contributed to ICHEP, Warsaw, Poland, 25-31, July 1996, Pr. No: PA10-019.

[26] K. Kiers and A. Soni, Phys. Rev D **56** (1997) 5786.

[27] M. Neubert, Modern. Phys. A **11** (1996) 4175.

[28] P. Ball and V. M. Braun, Phys. Rev D **49** (1994) 2472;
V. Eletsky and E. Shuryak, Phys. Lett B **276** (1992) 191;
M. Neubert, Phys. Lett B **322** (1994) 419.

[29] R. M. Barnett et al., Review of Particle Properties, Phys Rev D **54** (1996) 1.

[30] M. Acciarri et al. (L3 Collaboration), Phys. Lett. B **363** (1995) 127.

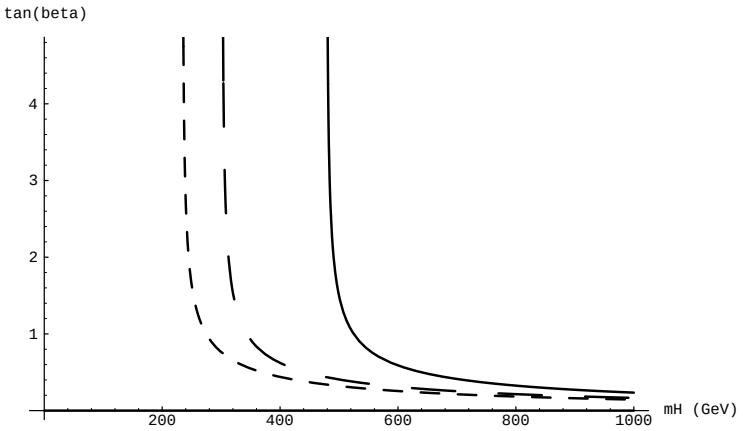

Figure 1: $tan\beta$ as a function of the mass m_H for fixed $C_7^{eff} = -0.4049$ in the model II of the 2HDM. Here solid curves correspond to the scale $\mu = 2.5\ GeV$, dashed curves to $\mu = 5\ GeV$ and small dashed curves to $\mu = 10\ GeV$.

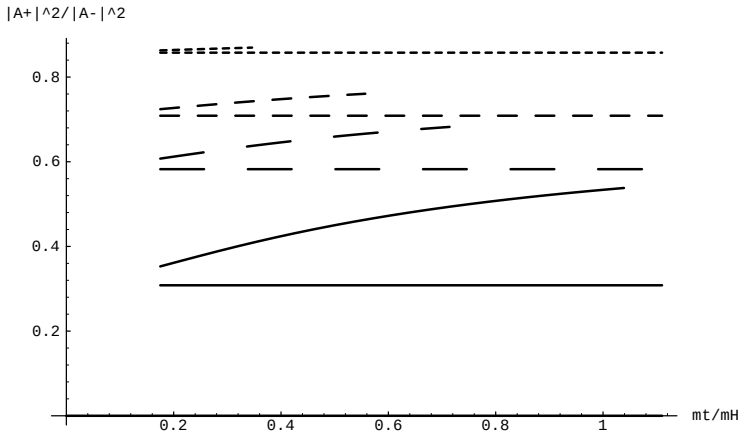

Figure 2: m_t/m_H dependence of the ratio $|A^+|^2/|A^-|^2$ for set 3 and $tan\beta = 2$. Here, solid lines (curves) correspond to the SM (model II 2HDM) at $\mu = m_W$, long dashed lines (curves) to SM (model II 2HDM) at $\mu = 10\ GeV$, medium dashed lines (curves) to SM (model II 2HDM) at $\mu = 5\ GeV$ and small dashed lines (curves) to SM (model II 2HDM) at $\mu = 2.5\ GeV$.

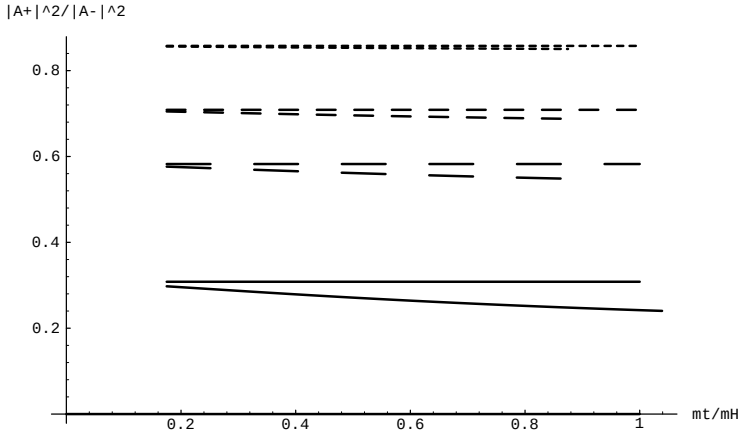

Figure 3: Same as fig 2, but in model I.

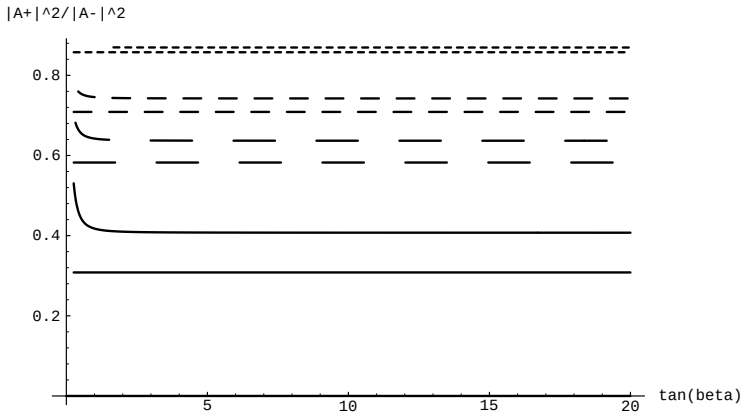

Figure 4: $tan\beta$ dependence of the ratio $|A^+|^2/|A^-|^2$ for set 3 for $m_H = 500\ GeV$. Here, solid lines (curves) correspond to the SM (model II 2HDM) at $\mu = m_W$, long dashed lines (curves) to SM (model II 2HDM) at $\mu = 10\ GeV$, medium dashed lines (curves) to SM (model II 2HDM) at $\mu = 5\ GeV$ and small dashed lines (curves) to SM (model II 2HDM) at $\mu = 2.5\ GeV$.

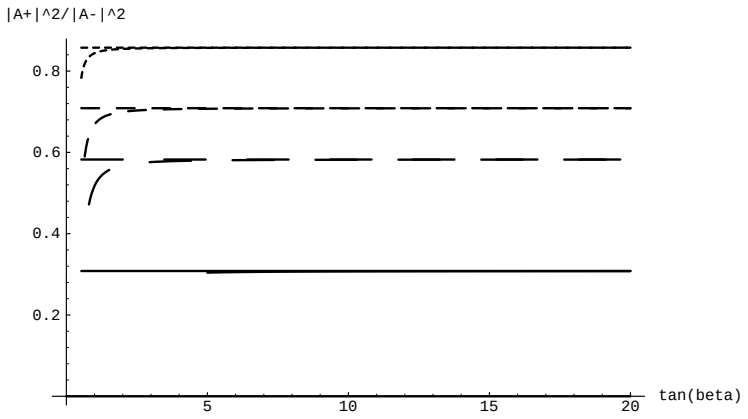

Figure 5: Same as fig 4, but in model I 2HDM.

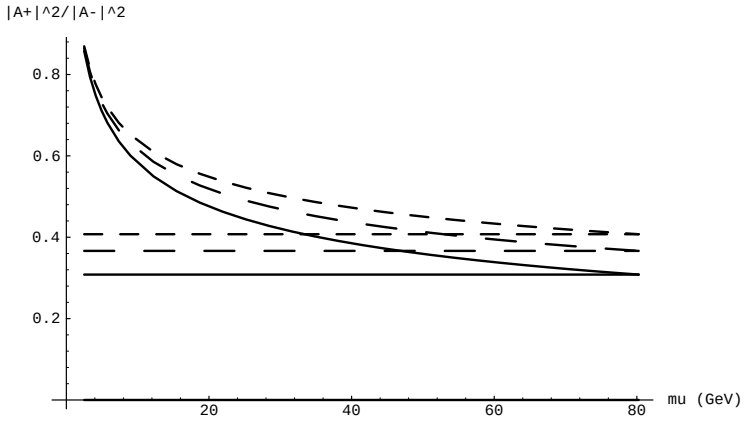

Figure 6: The scale dependence of the ratio $|A^+|^2/|A^-|^2$ for set 3 in the SM and for 2 values of $m_H = 500,\ 800\ GeV$ with $tan\beta = 10$. Here, solid lines (curves) correspond to the SM at $\mu = m_W$ (at arbitrary μ scale) , long dashed lines (curves) to model II with $m_H = 800\ GeV$ at $\mu = m_W$ (at arbitrary μ scale), and small dashed lines (curves) model II with $m_H = 500\ GeV$ at $\mu = m_W$ (at arbitrary μ scale).

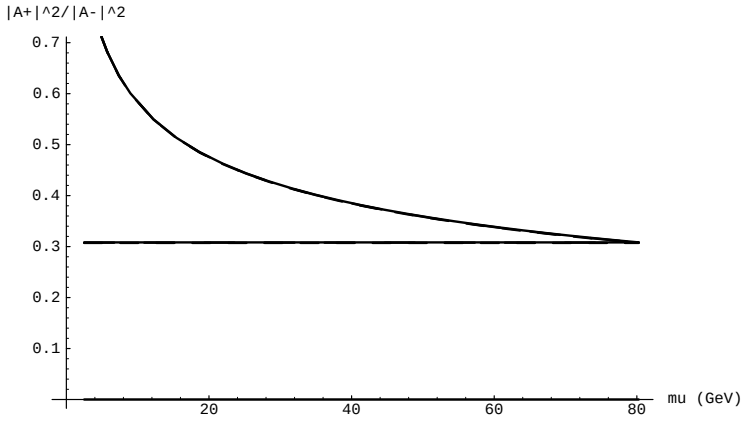

Figure 7: Same as fig 6, but for model I. All curves coincide within errors.

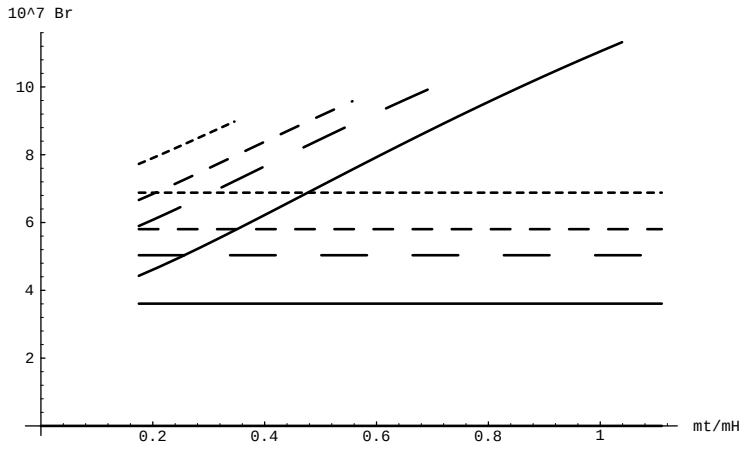

Figure 8: m_t/m_H dependence of the branching ratio Br for set 3 with $tan\beta = 2$. Here, solid lines (curves) correspond to the SM (model II 2HDM) at $\mu = m_W$, long dashed lines (curves) to the SM (model II 2HDM) at $\mu = 10\ GeV$, medium dashed lines (curves) to the SM (model II 2HDM) at $\mu = 5\ GeV$ and small dashed lines (curves) to the SM (model II 2HDM) at $\mu = 2.5\ GeV$.

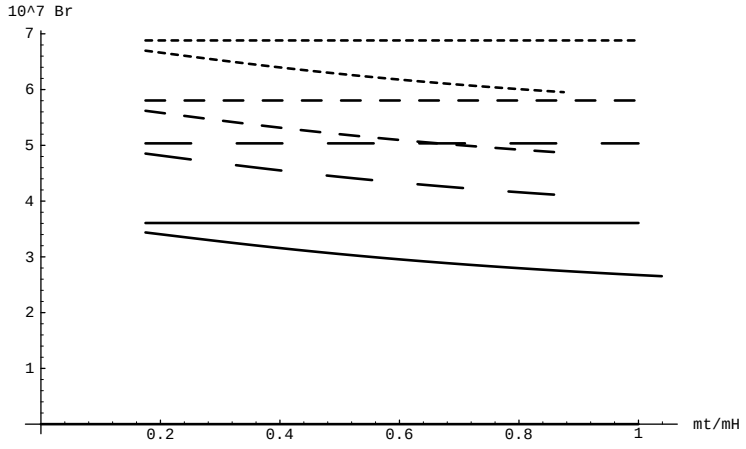

Figure 9: Same as fig 8, but in model I 2HDM.

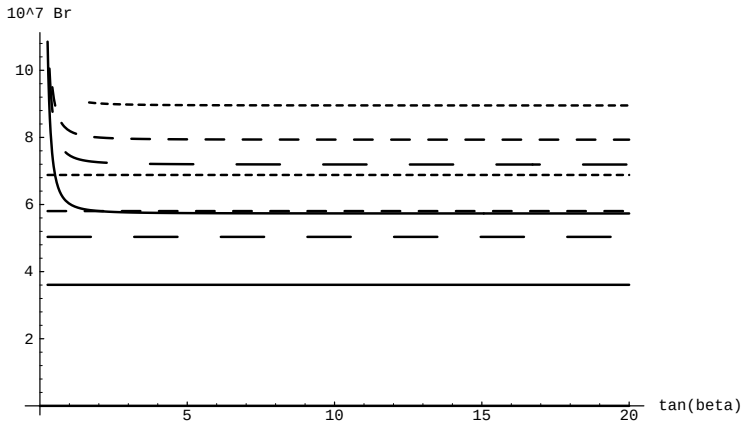

Figure 10: $tan\beta$ dependence of the Br for set 3 with $m_H = 500\ GeV$. Here, solid lines (curves) correspond to the SM (model II 2HDM) at $\mu = m_W$, long dashed lines (curves) to the SM (model II 2HDM) at $\mu = 10\ GeV$, medium dashed lines (curves) to the SM (model II 2HDM) at $\mu = 5\ GeV$ and small dashed lines (curves) to the SM (model II 2HDM) at $\mu = 2.5\ GeV$.

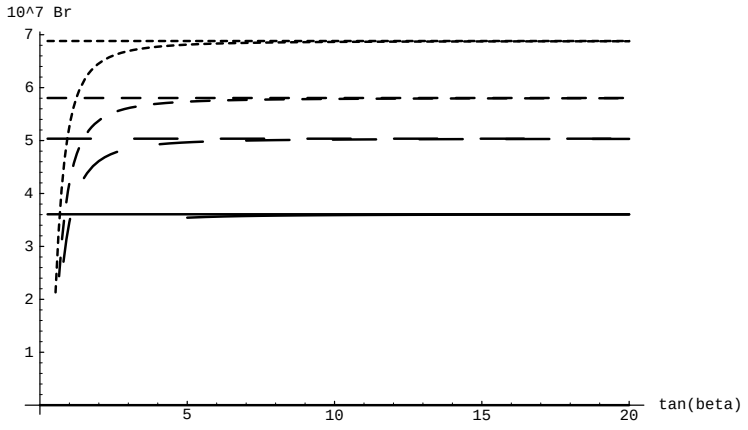

Figure 11: Same as fig 10, but in model I 2HDM.

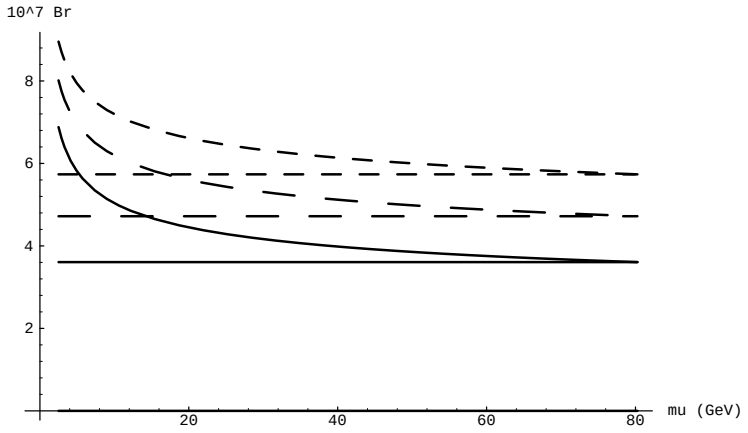

Figure 12: The scale dependence of the Br for set 3 and for 2 values of $m_H = 500,\ 800\ GeV$ with $tan\beta = 10$. Here, solid lines (curves) correspond to the SM at $\mu = m_W$ (at arbitrary μ scale), dashed lines (curves) to model II 2HDM with $m_H = 800\ GeV$ at $\mu = m_W$ (at arbitrary μ scale), and small dashed lines (curves) model II 2HDM with $m_H = 500\ GeV$ at $\mu = m_W$ (at arbitrary μ scale).

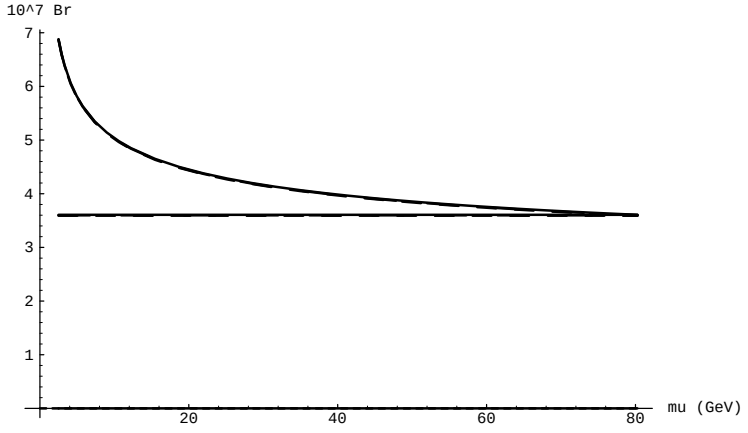

Figure 13: Same as fig 12, but for model I 2HDM. All curves coincide within errors.

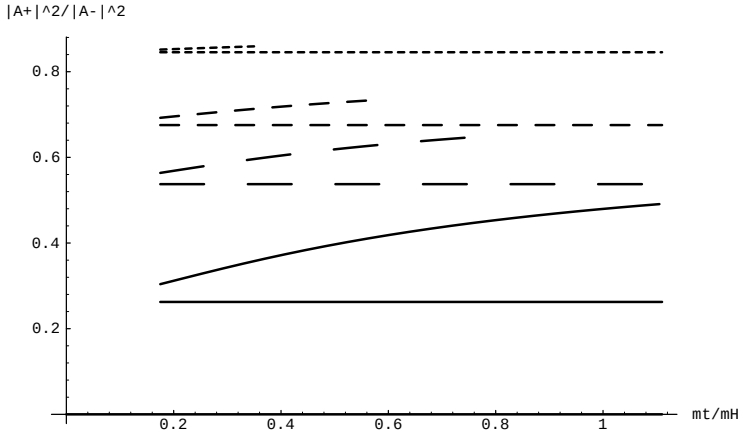

Figure 14: m_t/m_H dependence of the ratio $|A^+|^2/|A^-|^2$ for set 3 at $tan\beta = 10$ with the addition of LD_{O_7} effects. Here, solid lines (curves) correspond to the SM (model II 2HDM) at $\mu = m_W$, long dashed lines (curves) to the SM (model II 2HDM) at $\mu = 10\ GeV$, medium dashed lines (curves) to the SM (model II 2HDM) at $\mu = 5\ GeV$ and small dashed lines (curves) to the SM (model II 2HDM) at $\mu = 2.5\ GeV$.

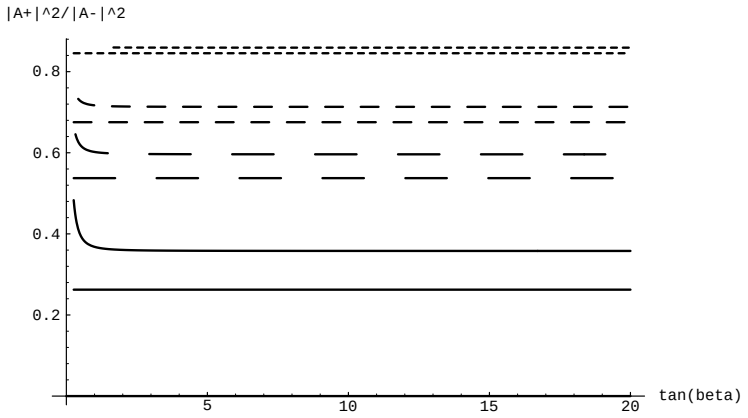

Figure 15: $tan\beta$ dependence of the ratio $|A^+|^2/|A^-|^2$ for set 3 for $m_H = 500\ GeV$ with the addition of LD_{O_7} effects. Here, solid lines (curves) correspond to the SM (model II 2HDM) at $\mu = m_W$, long dashed lines (curves) to the SM (model II 2HDM) at $\mu = 10\ GeV$, medium dashed lines (curves) to the SM (model II 2HDM) at $\mu = 5\ GeV$ and small dashed lines (curves) to the SM (model II 2HDM) at $\mu = 2.5\ GeV$.

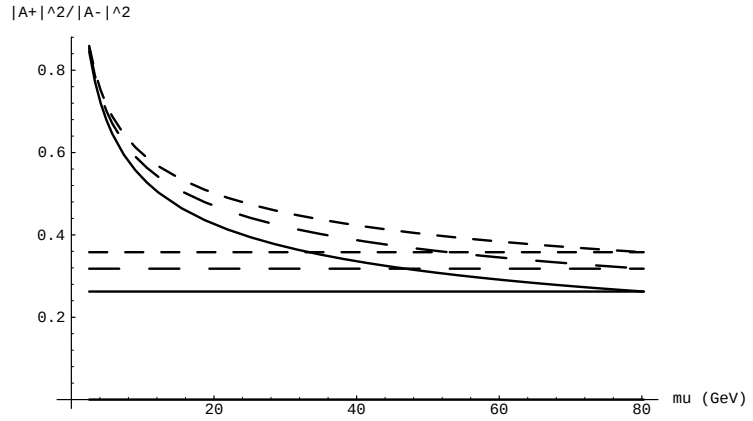

Figure 16: The scale dependence of the ratio $|A^+|^2/|A^-|^2$ for set 3 and for 2 values of $m_H =$ 500, 800 GeV at $tan\beta = 10$ with the addition of LD_{O_7} effects. Here, solid lines (curves) correspond to the SM at $\mu = m_W$ (at arbitrary μ scale), dashed lines (curves) to model II 2HDM with $m_H = 800\ GeV$ at $\mu = m_W$ (at arbitrary μ scale), and small dashed lines (curves) to model II 2HDM with $m_H = 500\ GeV$ at $\mu = m_W$ (at arbitrary μ scale).

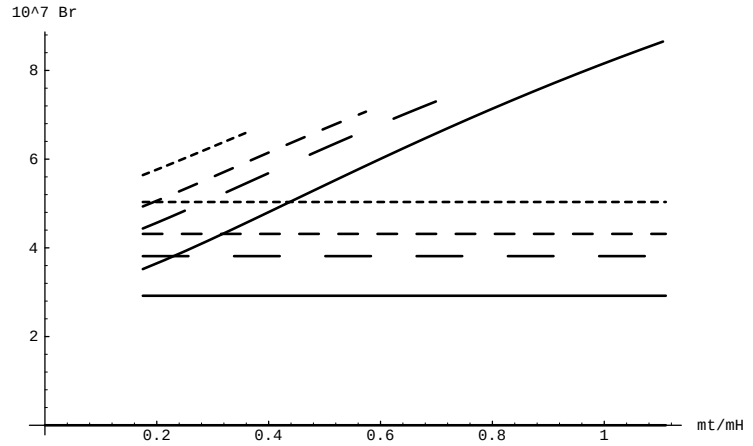

Figure 17: m_t/m_H dependence of the Br for set 3 at $tan\beta = 10$ including LD_{O_7} effects. Here, solid lines (curves) correspond to the SM (model II 2HDM) at $\mu = m_W$, long dashed lines (curves) to the SM (model II 2HDM) at $\mu = 10\ GeV$, medium dashed lines (curves) to the SM (model II 2HDM) at $\mu = 5\ GeV$ and small dashed lines (curves) to the SM (model II 2HDM) at $\mu = 2.5\ GeV$.

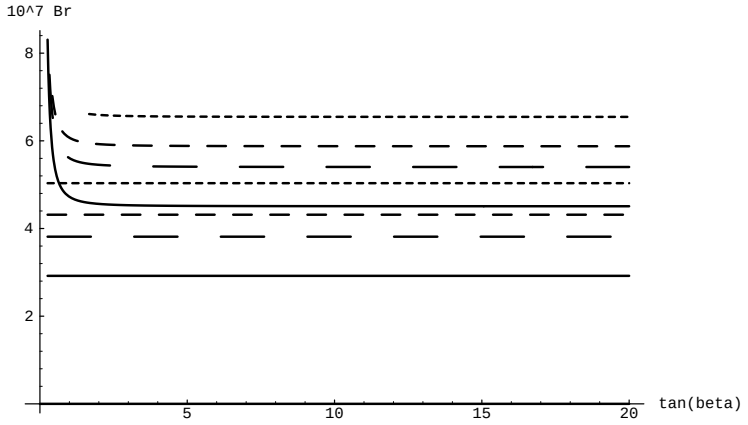

Figure 18: $tan\beta$ dependence of the Br for set 3 for $m_H = 500\ GeV$ including LD_{O_7} effects. Here, solid lines (curves) correspond to the SM (model II 2HDM) at $\mu = m_W$, long dashed lines (curves) to the SM (model II 2HDM) at $\mu = 10\ GeV$, medium dashed lines (curves) to the SM (model II 2HDM) at $\mu = 5\ GeV$ and small dashed lines (curves) to the SM (model II 2HDM) at $\mu = 2.5\ GeV$.

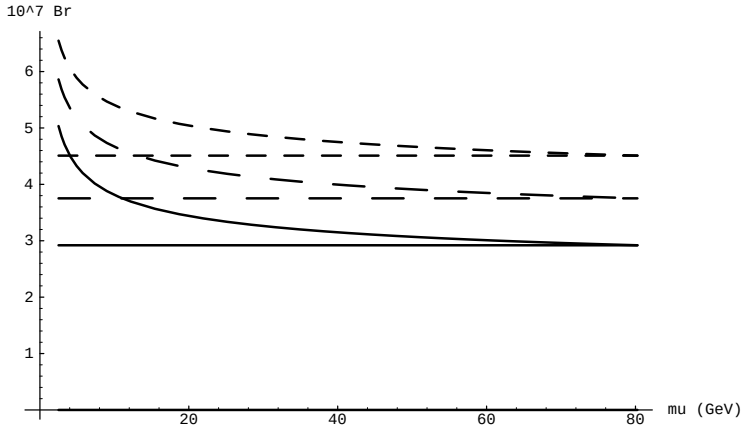

Figure 19: The scale dependence of the Br for set 3 and for 2 values of $m_H = 500,\ 800\ GeV$ at $tan\beta = 10$ including LD_{O_7} effects. Here, solid lines (curves) correspond to the SM at $\mu = m_W$ (at arbitrary μ scale), dashed lines (curves) to model II 2HDM with $m_H = 800\ GeV$ at $\mu = m_W$(at arbitrary μ scale) and small dashed lines (curves) to model II 2HDM with $m_H = 500\ GeV$ at $\mu = m_W$ (at arbitrary μ scale).